

Title: Analysis of Wave Profiles
for Single Crystal HMX

Author(s): R. MENIKOFF, rtm@lanl.gov
 J. J. DICK, jjd@lanl.gov
 D. E. HOOKS, dhooks@lanl.gov

Submitted to: Journal of Applied Physics

Analysis of Wave Profiles for Single Crystal HMX

Ralph Menikoff,* J. J. Dick, and D. E. Hooks

Los Alamos National Laboratory

Los Alamos, New Mexico 87545

(Dated: June 10, 2004)

Wave profiles measured in single crystal β -HMX (cyclo-tetramethylene-tetranitramine) display the characteristic response of an elastic-plastic material; an elastic precursor followed by a plastic wave. Moreover, the elastic precursor decays with the length of run. Numerical simulations with a rate-dependent elastic-plastic model are used to account for non-linear and transient wave behavior. In addition, to account for the measured anisotropy in propagation, parameters of an isotropic model are fit for two propagation directions; normal to the (011) and (010) planes of the $P2_1/n$ space group. Equation of state parameters are constrained by data for the longitudinal sound speed and hydrostatic compression. The fits show that the effective yield strength varies with direction from 0.18 GPa for the (011) orientation to 0.31 GPa in the (010) orientation.

PACS numbers: 62.20.Fe, 62.50.+p, 83.60.Uv

Keywords: HMX, elastic-plastic flow, shock wave

I. INTRODUCTION

Plastic-bonded explosives are a composite of explosive grains and binder. Initiation sensitivity is determined by hot spots or localized regions of high temperature. Hot spots are subgrain in extent. Consequently, simulations of hot-spot initiation require that individual grains are resolved. Calculations that resolve heterogeneities are known as meso-scale simulations (see *e.g.*, [1]). Clearly, they require constitutive properties of the explosive grains. Here we focus on the explosive HMX¹, in particular, the β -polymorph which is thermodynamically stable at ambient conditions. A single crystal of HMX is very insensitive [2] and can be treated as inert. Consequently, shock wave profiles can be used to infer mechanical properties.

Dick, Hooks *et al.*, [3] have performed a series of plate impact experiments and measured Lagrangian velocity time histories (VISAR² records) for ‘shock’ waves propagating in single crystal HMX. The experiments varied the length of the HMX sample, the orientation of the crystal (which are specified for the $P2_1/n$ space group) and the impact pressure. Wave profiles deduced from the time histories display the characteristic form associated with an elastic-plastic material, namely, a shock-like elastic precursor followed by a dispersed plastic wave. Moreover, the precursor decays with the distance of run, *i.e.*, length of sample. In addition, the profiles display a significant dependence on the direction of propagation.

A feature of the HMX wave profiles is that the particle velocity behind the elastic precursor is not monotonic. A similar behavior is observed for LiF [4]. In this case rate-dependent elastic-plastic constitutive laws have

been used to model the wave structure and the transient response of the elastic precursor [5, 6]. Here we use a similar elastic-plastic model to analyze the data for HMX.

The model assumes uniaxial flow and accounts for crystal anisotropy by letting the constitutive parameters vary with the direction of propagation. This simplification is used because the available data is not sufficient to develop a fully anisotropic model; limited data on the directional dependence of the sound speed only partially determines the stiffness tensor [7], and the two slip systems that have been clearly identified are insufficient to determine the yield surface. A consequence of assuming isotropic constitutive properties for uniaxial flow is that the model only accounts for longitudinal waves and imposes a free slip boundary condition at material interfaces.

Key model parameters include the yield strength, shear modulus and time constant associated with the plastic strain rate. These parameters are determined by fitting simulated wave profiles to the experimental data. The resulting yield strengths are 0.18 and 0.31 GPa for the directions normal to the (011) and (010) planes, respectively. The corresponding shear moduli are 11 and 7 GPa. It should be noted that the transient wave behavior leads to a strong nonlinear dependence of the profiles on the model parameters. This results in large uncertainties for the values of the parameters, tens of per cent. Nevertheless, it is clear that the anisotropic response exhibited by HMX is significant.

The time constant associated with the plastic wave width varies with wave strength. It is on the order of 50 ns for shock pressures on the order of 1 GPa. This corresponds to an effective viscosity in the range of 10 to 100 Pa s. We note that viscous coefficients within this range are required for hot-spot models based on viscosity as the dominant dissipative mechanism [8, 9].

The elastic-plastic model and the fitting parameters for HMX are described in section 2. The parameters are constrained by the measured values of the longitudinal sound speeds [3] and hydrostatic compression data

*Electronic address: rtm@lanl.gov

¹ Cyclo-tetramethylene-tetranitramine, C₄H₈N₈O₈.

² Velocity Interferometry System for Any Reflector.

[10, 11]. Simulated results and a comparison with the experimental data are presented in section 3. Incorporating the anisotropic response of an HMX grain into meso-scale initiation simulations for a plastic-bonded explosive is discussed in the last section.

II. ELASTIC-PLASTIC MODEL

A. Uniaxial Flow

Uniaxial rate-dependent elastic-plastic flow for an isotropic material is described by the partial differential equations

$$\begin{aligned} \frac{\partial}{\partial t}(\rho) + \frac{\partial}{\partial x}(\rho u) &= 0 \\ \frac{\partial}{\partial t}(\rho u) + \frac{\partial}{\partial x}(\rho u^2 - \sigma^{xx}) &= 0 \\ \frac{\partial}{\partial t}(\rho E) + \frac{\partial}{\partial x}(\rho E u - \sigma^{xx} u) &= 0 \quad (1) \\ \hline \frac{\partial}{\partial t}(\rho \epsilon_{\text{pl}}) + \frac{\partial}{\partial x}(\rho u \epsilon_{\text{pl}}) &= \rho \mathcal{R}_1 \\ \frac{\partial}{\partial t}(\rho \tau^{-1}) + \frac{\partial}{\partial x}(\rho u \tau^{-1}) &= \rho \mathcal{R}_2 \tau^{-1} \end{aligned}$$

where ρ is the mass density, u is the particle velocity, e is the internal specific energy, $E = \frac{1}{2}u^2 + e$ is the total specific energy, σ^{xx} is the longitudinal component of the stress tensor, ϵ_{pl} is the plastic strain variable and τ is a time constant for the plastic strain rate. The rates are only non-zero in the plastic regime, $|\epsilon_{\text{el}}| > \epsilon_{\text{y,el}}$. We take them to have the form

$$\begin{aligned} \mathcal{R}_1 &= -(\epsilon_{\text{pl}} - \epsilon_{\text{y,pl}})\tau^{-1}, \\ \mathcal{R}_2 &= \frac{[(\epsilon_{\text{pl}} - \epsilon_{\text{y,pl}})/\epsilon_{\text{y,el}}]^{n_1}}{\tau_1}. \quad (2) \end{aligned}$$

where $\epsilon_{\text{y,el}}$ is the elastic shear strain on the yield surface, $\epsilon_{\text{y,pl}} = \ln(\rho_0/\rho) - \epsilon_{\text{y,el}}$ is the plastic strain on the yield surface, and τ_1 and n_1 are fitting parameters.

The plastic strain rate can be motivated by the Orowan relation for dislocation dynamics in a crystal, see *e.g.*, [12]. The use of an internal degree of freedom for the plastic time constant is associated with a dynamic equation for the increase in the dislocation density, see [6, 13]. It allows the model to fit the non-monotonic particle velocity behind the precursor of the measured wave profiles. We note that rate-dependent plasticity can be approximated by rate-independent plasticity plus a viscous stress with viscosity coefficient $\nu = G\tau$ where G is the shear modulus. Consequently, treating the plastic time constant as a dynamic variable has an effect similar to that of a rate-dependent viscous coefficient.

The fitting form chosen for the plastic rates has the property that the time integral (holding ρ and e fixed)

has an analytic solution

$$\begin{aligned} \tau^{-1} &= \left[1 + \frac{\tau_0}{n_1 \tau_1} \left(\frac{\Delta \epsilon_{\text{pl}}}{\epsilon_{\text{y,el}}} \right)^{n_1} E(\Delta t) \right] \tau_*^{-1} \\ \epsilon_{\text{pl}} &= \epsilon_{\text{y,pl}} - \left[\frac{\left[1 + \frac{\tau_0}{n_1 \tau_1} \left(\frac{\Delta \epsilon_{\text{pl}}}{\epsilon_{\text{y,el}}} \right)^{n_1} \right] E(\Delta t)}{1 + \frac{\tau_0}{n_1 \tau_1} \left(\frac{\Delta \epsilon_{\text{pl}}}{\epsilon_{\text{y,el}}} \right)^{n_1} E(\Delta t)} \right]^{1/n_1} \Delta \epsilon_{\text{pl}} \quad (3) \end{aligned}$$

where $\Delta \epsilon_{\text{pl}} = (\epsilon_{\text{pl}})_0 - \epsilon_{\text{y,pl}}$, $\Delta t = t - t_0$ and

$$\begin{aligned} \tau_*^{-1} &= \left[1 + \frac{\tau_0}{n_1 \tau_1} \left(\frac{\Delta \epsilon_{\text{pl}}}{\epsilon_{\text{y,el}}} \right)^{n_1} \right] \tau_0^{-1}, \\ E(\Delta t) &= \exp\left(\frac{-n_1 \Delta t}{\tau_*} \right). \quad (4) \end{aligned}$$

This enables an efficient hyperbolic solver, that accounts for source terms with an operator split algorithm, to be used for the simulations.

B. Constitutive Parameters

To ensure thermodynamic consistency, we use a hyper-elastic formulation in which the stress is the derivative of the energy with respect to the strain. We assume the energy is the sum of hydrostatic and shear components. The full three-dimensional model is greatly simplified when the flow is restricted to uniaxial strain. The reduction to uniaxial flow is described in [14]. We use the same formulation and to save space the formulas are not repeated here. We note that the model is specified by a hydrostatic pressure and a hydrostatic shear modulus G .

Data for HMX only partially determines the elastic tensor [7]. Instead of using a full anisotropic model, separate fits are used for the two directions of interest, normal to the (011) and (010) planes. The fits are constrained by hydrostatic compression data [10, 11], and the measured values of the longitudinal sound speed [3], 3.82 and 3.17 mm/ μ s for the (011) and (010) orientations, respectively. For the hydrostatic component of stress we use a Hayes EOS [16] based on a Birch-Murnaghan isotherm [17]. The Birch-Murnaghan fitting form has two parameters; initial bulk modulus K_0 and its pressure derivative K'_0 . For a chosen value of G_0 , the bulk modulus is determined by the longitudinal sound speed, $K_0 = \rho_0 c_{\text{long}}^2 - \frac{4}{3}G_0$. The parameter K'_0 is used to fit the hydrostatic compression data above the yield stress.

For a steady-state split elastic-plastic wave, the values of shear modulus G and the yield strength $Y = 2G\epsilon_{\text{y,el}}$ would be determined by the amplitude of the elastic precursor and the difference in elastic and plastic wave speeds. However, the HMX wave profiles display a strong transient behavior. Consequently, G and Y can not be determined independently of the plastic strain rate. The parameters are determined by matching simulated profiles to the experimental ones. The parameters that gave

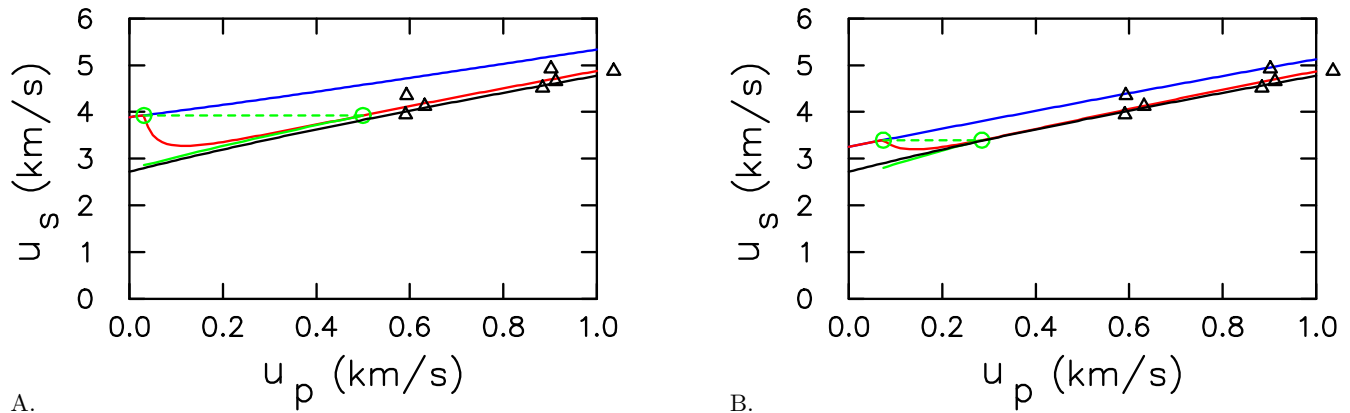


FIG. 1: Hugoniot loci for HMX; A. (011), and B. (010) orientations. The curves are as follows: blue is frozen (elastic) locus; red is equilibrium locus; solid green is plastic wave following elastic precursor; dashed green is Rayleigh line in 2 wave regime; black is locus for hydrostatic EOS [11]. The symbols are Hugoniot data for solvent pressed HMX [15, p. 596].

the best subjective match are listed in table I. The comparison with the wave profiles is presented in the next section. For the chosen parameters, the yield strengths are 0.18 and 0.31 GPa for the (011) and (010) orientation, respectively.

From the EOS, the principal Hugoniot can be computed. The Hugoniot loci in the (particle velocity, shock velocity)–plane for the two directions are shown in figure 1. We note that the extent of the elastic regime and the extent of the elastic-plastic regime are sensitive to the values of G and Y , and vary greatly for the two directions. The experiments measured profiles for waves with strengths $u_p \approx 0.28$ and 0.43 km/s. The lower strength wave is well within the elastic-plastic regime for both propagation directions. The stronger wave is in the elastic-plastic regime for the (011) orientation, but in the plastic regime for the (010) orientation. However, we will see that transient effects due to the plastic rate greatly affect the wave profiles.

TABLE I: Constitutive parameters for HMX

	(011)	(010)	units
K_0	13.0	9.75	GPa
K'_0	10.5	15.	—
G	11.0	7.0	GPa
$\epsilon_{y,e}$	0.008	0.022	—
τ_0^{-1}	2.	0.02	μs^{-1}
n_1	1.5	1.5	—
τ_1	0.035	0.006	μs
	$\rho_0 = 1.9 \text{ g/cm}^3$		
	$\Gamma/V = 1.1 \text{ g/cm}^3$		

III. SIMULATIONS

Simulations of experiments were performed using an adaptive mesh Lagrangian algorithm (second order Godunov scheme) within the Am³ environment of James Quirk [18–20]. Am³ is available on line [21], and the EOS plugin and scripts to generate the numerical results on a Linux PC are available on request from the author.

A schematic of the experiments of Dick, Hooks *et al.*, [3, Fig. 1] is shown in figure 2. The simulations included the anvil, the HMX sample and the PMMA³ window. The anvil is x-cut quartz for the low pressure waves (1.4 GPa) and Kel-F⁴ for the high pressure waves (2.4 GPa). A Mie-Grüneisen EOS with the prin-

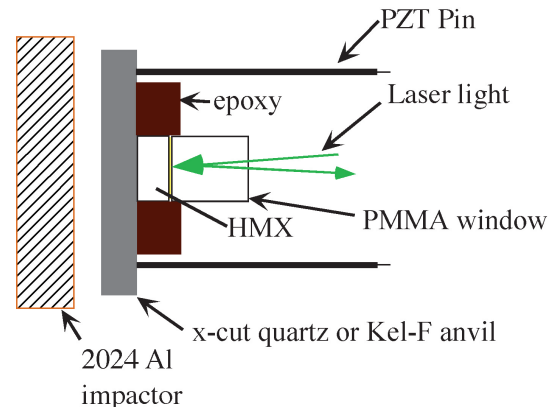


FIG. 2: Schematic of wave profile experiments of Dick, Hooks *et al.*, [3, Fig. 1]. VISAR data corresponds to the Lagrangian time history of the HMX/PMMA interface.

³ polymethyl methacrylate
⁴ polychlorotrifluoroethylene

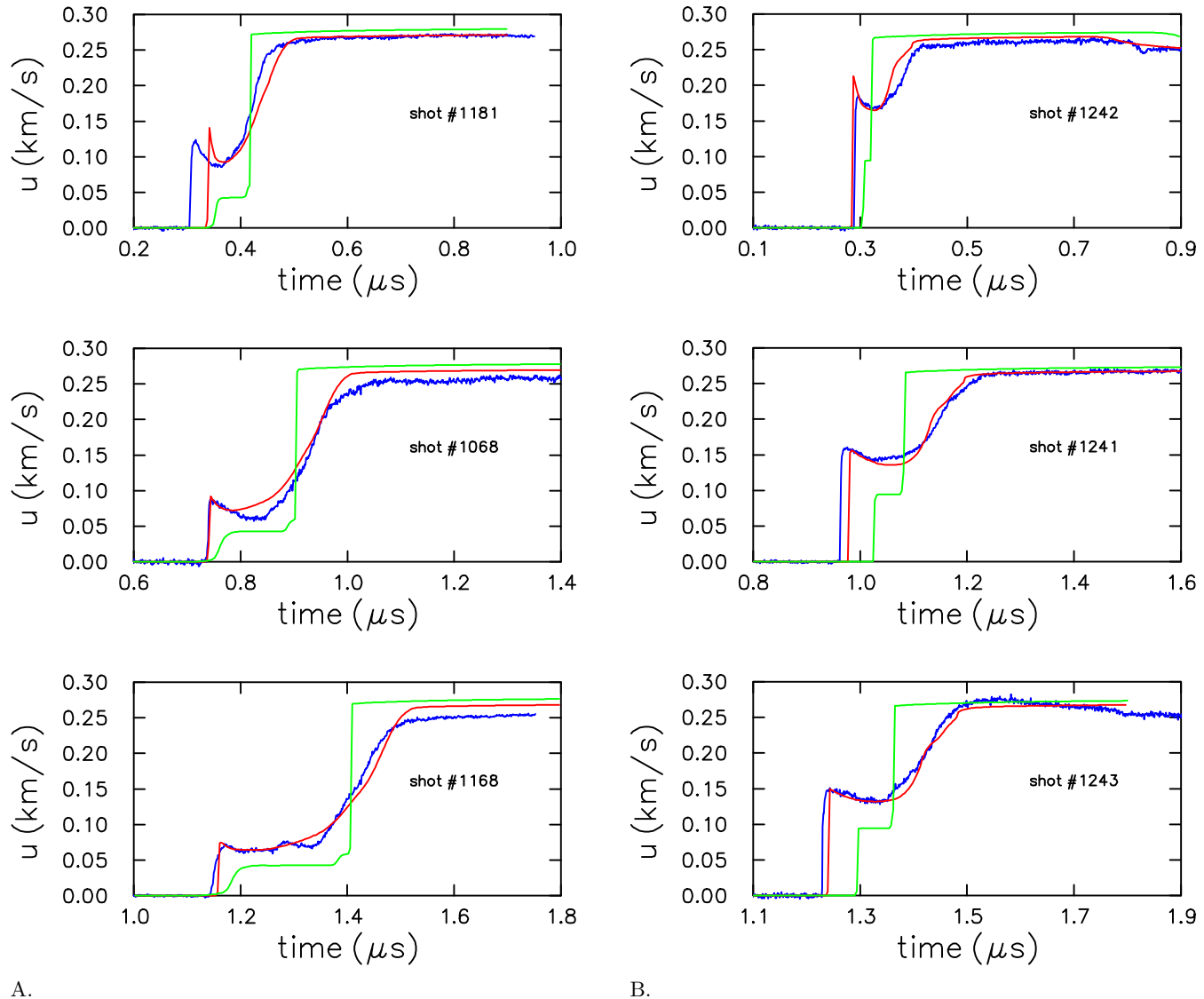


FIG. 3: Comparison with VISAR data for shock pressure of 1.4 GPa. A. (011) orientation with sample lengths of 1.39, 3.00 and 4.66 mm; shot numbers 1181, 1068, 1168, respectively. B. (010) orientation with sample lengths of 1.04, 3.49 and 4.40 mm; shot numbers 1242, 1241, 1243, respectively. Blue curve is experimental data [3]. Red and green curves are simulations with elastic-plastic model for rate-dependent and rate-independent plasticity, respectively.

cipal Hugoniot as the reference curve is used for these material. The Hugoniot is determined by a linear $u_s - u_p$ relation; for x-cut quartz [22] $u_s = 5.72 + 0.01u_p$ km/s, and for Kel-F [15, pp. 434–435], $u_s = 2.03 + 1.64u_p$ km/s. An elastic-plastic constitutive model is used for the PMMA [14].

The parameters for the experiments, identified by shot number, are given in [3, table I]. The initial shock state in the anvil is determined by an impedance match using the measured impactor velocity. For the aluminum impactor a Mie-Grüneisen EOS is used with [15, pp. 166–172] $u_s = 5.37 + 1.29u_p$ km/s. The shock state in the anvil is used to set the initial conditions that drive the simulations. The time origin is based on the PZT pins (see fig. 2) and corresponds to the start of the wave in

the HMX sample. No arbitrary adjustments of either the wave strength or the time origin are used in the comparisons with experiments.

A. 1.4 GPa Shock Pressure

Constitutive parameters of HMX are fit for two orientations, (011) and (010), based on 3 experiments each with different sample lengths and a shock pressure of 1.4 GPa. The comparison of the VISAR data between the experiment and simulation for the ‘best’ fit is shown in figure 3. It is difficult to come up with a quantitative measure for the difference of the profiles that adequately accounts for systematic errors, such as arrival time of the

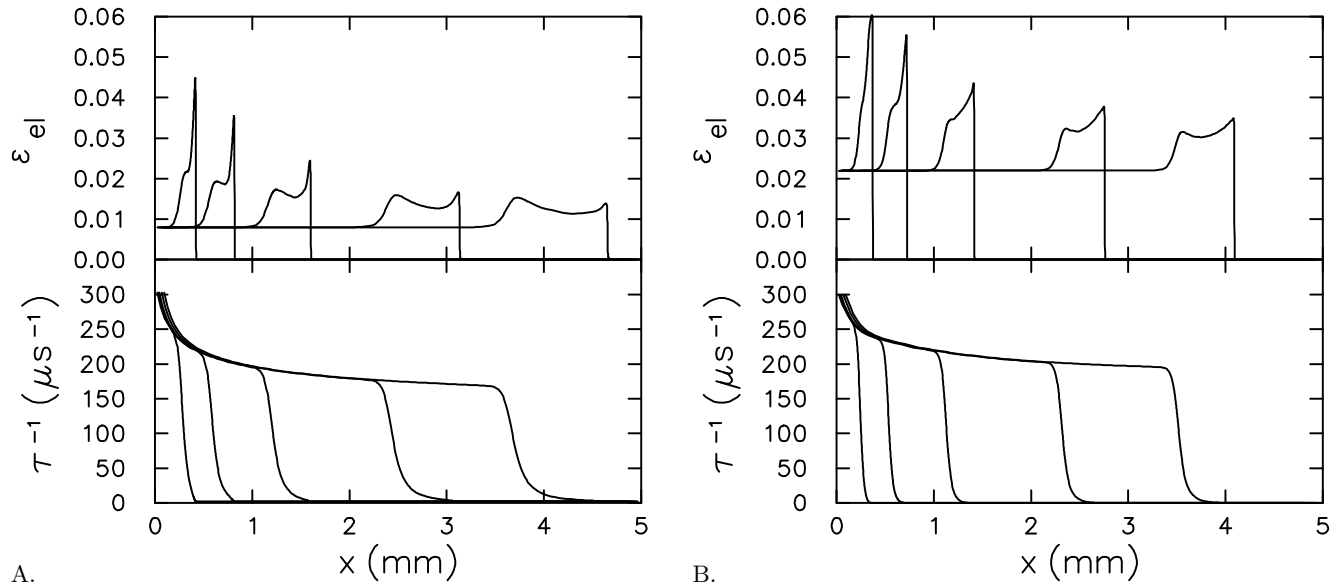


FIG. 4: Time evolution of profiles for elastic shear-strain and inverse plastic time constant; A. (011), and B. (010) orientation. Profile times are 0.1, 0.2, 0.4, 0.8, 1.2 μs .

lead wave and final amplitude, and weights important qualitative features, such as the velocity decrease behind the precursor. Consequently, the best fit is necessarily subjective.

Figure 3 also shows simulated profiles for rate-independent plasticity. These profiles represent the asymptotic strength of the elastic and plastic waves based on the equation of state and corresponds to the limit of zero relaxation time constant. Both the data and rate-dependent plastic simulations differ significantly from the rate-independent case. The amplitude and arrival time of the precursor are affected by its transient decay. The arrival time of the plastic wave is affected by changes of the conserved quantities (mass, momentum and energy) within its profile. As a consequence of the strong transient behavior, even after 4.5 mm of run, the fitting parameters are not linearly independent. This results in large uncertainties of the fit. Nevertheless, it is clear from the profiles for the two orientations that HMX exhibits a significant anisotropy. The best estimate for the yield strengths are 0.18 and 0.31 GPa for the directions normal to the (011) and (010) planes, respectively. The corresponding shear moduli are 11 and 7 GPa.

VISAR data represents a Lagrangian time history at the sample-window interface, see fig. 2. The simulations show that the impedance mismatch results in a reflected rarefaction into the HMX. The release wave quenches the plastic strain rate. Both HMX and PMMA support shear stress. The uniaxial flow model assumes free slip at the interface. As a consequence, the simulated flow shows a discontinuity in the shear stress at the interface. Moreover, no transverse waves are generated by the impedance mismatch. These effects are folded into the VISAR data.

Wave profiles at fixed times can easily be computed

for HMX only. These are unaffected by the impedance mismatch between the HMX and PMMA. Elastic shear-strain profiles, for both orientations, are shown in figure 4. The time evolution of these profiles clearly shows the decay of the elastic precursor. In addition, the profiles for the inverse plastic time constant τ^{-1} are shown. In the region of the plastic profile, $\tau^{-1} \approx 160$ and $200 \mu\text{s}$, for the (011) and (010) orientations respectively. For the 1.4 GPa plastic wave, the wave width corresponds to an effective viscosity $\nu = G\tau = 65$ and $35 \text{ Pa}\cdot\text{s}$, respectively. Due to the dynamics of the plastic strain, the time constant, and hence the effective viscosity, decreases as the wave strength is increased.

B. 2.4 GPa Shock Pressure

As a check on the fit, the same parameters were used to simulate the experiments for the 2.4 GPa waves. The comparison with the VISAR data is shown in figure 5. Though the simulated profiles are semi-quantitative, there is 50 ns difference in the arrival time of the wave. This exceeds the $\pm 12 \text{ ns}$ experimental uncertainty of the time origin [3].

It can be seen from the rate-independent profile that the (010) orientation lies in the plastic regime. That is to say, the plastic wave outruns the elastic wave and there is no precursor. Nevertheless the rate-dependent simulations show a precursor. This indicates that the transient rate-dependent effects are important for the experimental distance of run. Without a theory as a guide for the form of the plastic strain rate, it is difficult to fit profiles over a wide range of cases.

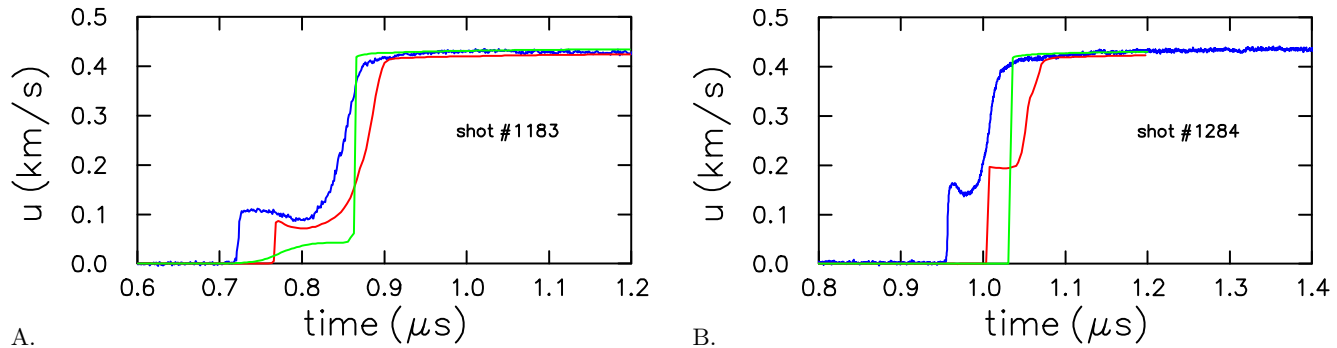


FIG. 5: Comparison with VISAR data for shock pressure of 2.4 GPa. A. (011) orientation with sample length of 3.11 mm (shot #1183), and B. (010) orientation with sample length of 3.65 mm (shot #1248). Blue curve is experimental data [3]. Red and green curves are simulations with elastic-plastic model for rate dependent and rate independent plasticity, respectively.

IV. CONCLUDING REMARKS

It is worthwhile to indicate how the model for HMX constructed here might be used in meso-scale simulations of initiation. Simulations of plastic-bonded explosive (PBX) to date have accounted for heterogeneities from the constituent materials; explosive, binder and void. Since explosive grains are crystalline, an additional source of heterogeneities is from the anisotropy of a crystal. Because of variations of the anisotropic response from crystal orientation, compressive waves give rise to fluctuations of the shear stress that can trigger sliding between grains or generate shear bands. The heating associated with these localized effects may be a significant source of hot spots [8] in the regime of weak initiation.

The generation of shear bands is usually associated with an instability resulting from the decrease of shear viscosity with temperature. We note that rate-dependent plasticity can have a similar behavior. There are two regimes for plastic strain rates based on dislocation motion [12]; weak shear is thermally activated and strong shear is drag dominated. The thermally activated regime can be approximated with a temperature dependent viscosity. The HMX model used here tacitly is assuming the drag dominated regime for the plastic strain by neglecting the temperature dependence of the plastic time constant.

As mentioned in the introduction, building in the full elastic-plastic anisotropy would be difficult. However, a large part of the effect could be incorporated within the context of an isentropic model by varying the equation of state from grain to grain to account for the variations in acoustic speeds and yield strength with crystal orientation. In effect, this corresponds to varying the parameters with orientation, as has been done here in fitting the experimental wave profiles.

Coarse grain HMX used in plastic-bonded explosives has an average diameter of about 0.14 mm. This is over an order of magnitude smaller than the sample lengths (up to 4.5 mm) used in the wave profile experiments. Consequently, the wave profile for a PBX would not be expected to have well separated elastic and plastic waves. However, the width of the wave would be determined largely by the relaxation time constant for the plastic strain in the crystalline grains.

The relaxation time constant is affected by defects in the crystal. The wave profile experiments use high quality crystals in order to obtain reproducible results. Plastic-bonded explosives are manufactured by pressing molding powder; explosive grains coated with binder. Pressing pressure are typically in the range of 20,000 psi or 0.14 GPa. This is comparable to the yield strength and one would expect the grains in a PBX to have many more defects than the crystals used in the wave profile experiments. Consequently, the relaxation time for a PBX would be smaller than obtained here by fitting to single crystal wave profiles.

We note that rise times have been measured for compaction waves in granular HMX. The rise times vary with porosity and grain size [23, Fig. 2.9]. But for shocks strengths of about 1 GPa, the rise time saturates at about 100 ns. Both the shock strength and rise time are comparable to those for the single crystal wave profiles considered here. This suggests that plasticity is important for granular HMX as well as a single crystal.

Acknowledgments

This work was carried out under the auspices of the U. S. Dept. of Energy at LANL under contract W-7405-ENG-36.

[1] M. R. Baer, *Thermochimica Acta* **384**, 351 (2002).

[2] A. W. Campbell and J. R. Travis, in *Proceedings of*

- Eighth Symposium (International) on Detonation, Albuquerque, NM, July 15–19, 1985* (Naval Surface Weapons Center, White Oak, Silver Spring, Maryland 20903–5000, 1986), pp. 1057–1068.
- [3] J. J. Dick, D. E. Hooks, R. Menikoff, and A. R. Martinez, submitted to *J. Appl. Phys.* (2004), URL <http://t14web.lanl.gov/Staff/rsm/preprints.html#HMxprofiles>.
- [4] Y. M. Gupta, G. E. Duvall, and G. R. Fowles, *J. Appl. Phys.* **46**, 532 (1975).
- [5] J. N. Johnson and O. E. Jones, *J. Appl. Phys.* **41**, 2330 (1970).
- [6] Y. Partom, *J. Appl. Phys.* **59**, 2716 (1986).
- [7] J. M. Zaug, in *Proceedings of the Eleventh Detonation Symposium* (1998).
- [8] R. B. Fry, in *Seventh (International) Symposium on Detonation* (1981), pp. 36–42.
- [9] B. A. Khasainov, A. A. Borisov, B. S. Ermolaev, and A. I. Korotkov, in *Seventh (International) Symposium on Detonation* (1981), pp. 435–447.
- [10] C. Yoo and H. Cynn, *J. Chem. Phys.* **111**, 10229 (1999).
- [11] R. Menikoff and T. D. Sewell, *High Pressure Research* **21**, 121 (2001).
- [12] J. N. Johnson, in *High-Pressure Shock Compression of Solids*, edited by J. R. Asay and M. Shahinpoor (Springer-Verlag, 1993), chap. 7, pp. 217–264.
- [13] J. N. Johnson and R. W. Rohde, *J. Appl. Phys.* **42**, 4171 (1971).
- [14] R. Menikoff, submitted to *J. Appl. Phys.* (2004), URL <http://t14web.lanl.gov/Staff/rsm/preprints.html#PMMA>.
- [15] S. Marsh, ed., *LASL Shock Hugoniot Data* (Univ. Calif. press, 1980), URL <http://lib-www.lanl.gov/books/shd.pdf>.
- [16] S. A. Sheffield, D. E. Mitchell, and D. B. Hayes, in *Sixth (International) Symposium on Detonation* (1976), pp. 748–754.
- [17] T. D. Sewell and R. Menikoff, in *Shock Compression in Condensed Matter – 2003* (2003), URL <http://t14web.lanl.gov/Staff/rsm/preprints.html#betaHMx>.
- [18] J. J. Quirk, in *29th Computational Fluid Dynamics* (von Karmen Institute, 1998), VKI Lecture Series, chap. 4, URL http://www.galcit.caltech.edu/~jjq/vki/vki:cf29::jjq_11.ps.gz.
- [19] J. J. Quirk, in *29th Computational Fluid Dynamics* (von Karmen Institute, 1998), VKI Lecture Series, chap. 5, URL http://www.galcit.caltech.edu/~jjq/vki/vki:cf29::jjq_12.ps.gz.
- [20] R. Menikoff and J. J. Quirk, Tech. Rep. LA-UR-01-6222, Los Alamos National Lab. (2001), URL <http://t14web.lanl.gov/Staff/rsm/preprints.html#EOSpackage>.
- [21] J. Quirk, *Amrita installation kit*, <http://www.amrita-ebook.org/download> (2003), see also, <http://www.amrita-ebook.org>.
- [22] G. E. Ingram and R. A. Graham, in *Proceedings of the Fifth Detonation Symposium* (1970), pp. 369–386.
- [23] S. A. Sheffield, R. L. Gustavsen, and M. U. Anderson, in *High-Pressure Shock Compression of Solids IV: Response of Highly Porous Solids to Shock Compression*, edited by L. Davison, Y. Horie, and M. Shahinpoor (Springer-Verlag, 1997), chap. 2, pp. 23–61.